Published in final edited form as:

Dev Dyn. 2021 April ; 250(4): 562–573. doi:10.1002/dvdy.259.

Tissue-specific analysis of *Fgf18* gene function in palate development

Minghui Yue[1], **Yu Lan**[1,2,3,4], **Han Liu**[1], **Zhaoming Wu**[1], **Toru Imamura**[5], **Rulang Jiang**[1,2,3,4,*]

[1]Division of Developmental Biology, Cincinnati Children's Hospital Medical Center, Cincinnati, OH 45229, USA;

[2]Division of Plastic Surgery, Cincinnati Children's Hospital Medical Center, Cincinnati, OH 45229, USA;

[3]Departments of Pediatrics and Surgery, University of Cincinnati College of Medicine, Cincinnati, OH 45229, USA;

[4]Shriners Hospitals for Children, Cincinnati, OH 45229, USA;

[5]Cell Regulation Laboratory, School of Bioscience and Biotechnology, Tokyo University of Technology, Hachioji, Tokyo 192-0982, Japan.

Abstract

Background: Previous studies showed that mice lacking Fgf18 function had cleft palate defects and that the *FGF18* locus was associated with cleft lip and palate in humans, but what specific roles Fgf18 plays during palatogenesis are unclear.

Results: We show that *Fgf18* exhibits regionally restricted expression in developing palatal shelves, mandible, and tongue, during palatal outgrowth and fusion in mouse embryos. Tissue-specific inactivation of *Fgf18* throughout neural crest-derived craniofacial mesenchyme caused shortened mandible and reduction in ossification of the frontal, nasal, and anterior cranial base skeletal elements in $Fgf18^{c/c}$;*Wnt1-Cre* mutant mice. About 64% of $Fgf18^{c/c}$;*Wnt1-Cre* mice exhibited cleft palate. Whereas palatal shelf elevation was impaired in many $Fgf18^{c/c}$;*Wnt1-Cre* embryos, no significant difference in palatal cell proliferation was detected between $Fgf18^{c/c}$;*Wnt1-Cre* embryos and their control littermates. Embryonic maxillary explants from $Fgf18^{c/c}$;*Wnt1-Cre* embryos showed successful palatal shelf elevation and fusion in organ culture similar to the maxillary explants from control embryos. Furthermore, tissue-specific inactivation of *Fgf18* in the early palatal mesenchyme did not cause cleft palate.

Conclusion: These results demonstrate a critical role for *Fgf18* expression in the neural crest-derived mesenchyme for the development of the mandible and multiple craniofacial bones but *Fgf18* expression in the palatal mesenchyme is dispensable for palatogenesis.

Keywords

bone; cleft palate; conditional gene knockout; neural crest; mouse

[*]Author for correspondence: Rulang Jiang, Ph.D., Division of Developmental Biology, Cincinnati Children's Hospital Medical Center, Cincinnati, OH 45229, USA. Telephone: 1-513-636-3212. Rulang.Jiang@cchmc.org.

1 Introduction

Development of the secondary palate begins on embryonic day (E) 11 in mice, which is corresponding to the 6th week of human development.[1] The primordia of the palatal shelves (PS) emerge from the oral side of the maxillary processes, grow vertically, and occupy the position lateral to the tongue until E14 to E14.5 when the PS reorient to the horizontal position above the tongue.[2] Further growth of PS ensures the attachment and fusion of opposing PS at the midline as well as fusion with the primary palate anteriorly and with the nasal septum dorsally. Further differentiation of palatal mesenchyme cells generates the palatal processes of the maxillary and palatine bones of the hard palate. Upon completion of palatogenesis, the initial oronasal cavity is subdivided into a nasal and an oral cavity. Any defect in the palatogenesis process might result in cleft palate (CP). In addition, impaired development of other oral and craniofacial components can also cause CP since secondary palate development occurs in concert with the development of those structures.[2]

The growth of PS is regulated by reciprocal signaling interactions between the palatal epithelium and the neural crest-derived palatal mesenchyme.[2] The secreted protein Sonic Hedgehog (Shh) is expressed in the palatal epithelium and signals to the palatal mesenchyme through activating the transmembrane protein Smoothened (Smo). Tissue-specific inactivation of *Shh* in the developing epithelium in *K14-Cre; Shh*$^{c/n}$ embryos caused a reduction in epithelial and mesenchyme proliferation and resulted in CP,[3] while *in vitro* cultures showed that Shh stimulated PS mesenchymal proliferation.[4] Tissue-specific inactivation of *Smo* in cranial neural crest cells resulted in the complete absence of secondary palate structures in the *Smo*$^{c/n}$*; Wnt1-Cre* mutant mouse embryos.[5] In contrast, epithelial loss of function of *Smo* did not result in CP, implying that the PS mesenchyme is the major target for Shh action during palate development.[4] Tissue-specific inactivation of *Smo* in the developing palatal mesenchyme caused significant reduction in PS mesenchyme proliferation, resulting in cleft palate in *Osr2*^{IresCre}*;Smo*$^{c/c}$ mice.[3] *Fgf10*, encoding a mitogenic growth factor of the fibroblast growth factor (FGF) family, is expressed in the developing palatal mesenchyme and is a target of Shh signaling.[3,4] Fgf10 signals to the palatal epithelium through the Fgfr2b receptor to maintain *Shh* expression, resulting in a positive feedback loop coordinating palatal epithelial and mesenchyme proliferation.[4] In addition to *Fgf10*, *Fgf7* and *Fgf18* are expressed in the developing palatal mesenchyme.[6–8] In contrast to the function of Fgf10, however, both Fgf7 and Fgf18 have been shown to inhibit *Shh* expression in the palatal epithelium in palatal explant culture assays.[6,8] Xu et al. (2016) identified a Shh-Foxf-Fgf18-Shh regulatory circuit in which the Foxf1 and Foxf2 transcription factors act downstream of Shh signaling to restricted *Fgf18* expression in the palatal mesenchyme during PS growth. On the other hand, mice lacking Fgf18 function died shortly after birth, with most of the *Fgf18*$^{-/-}$ pups exhibiting cleft palate.[9] *Fgf18*$^{-/-}$ pups also exhibited delayed ossification of both cranial and appendicular bones.

In this study, we use an *Fgf18* conditional knock-out mouse model to study the role of Fgf18 in palate development. Tissue-specific inactivation of *Fgf18* in premigratory neural crest cells in the *Fgf18*$^{c/c}$*;Wnt1-Cre* embryos caused cleft palate in association with hypoplastic craniofacial bones including reduced mandible. Whereas many *Fgf18*$^{c/c}$*;Wnt1-Cre* embryos exhibited failure of PS elevation, the *Fgf18*$^{c/c}$*;Wnt1-Cre* mutant maxillary explants,

dissociated from the mandible and tongue, exhibited PS elevation and fusion similar to the control explants in culture. Furthermore, we demonstrate that tissue-specific inactivation of *Fgf18* in palatal mesenchyme cells did not disrupt palatogenesis, indicating that *Fgf18* expression in the palatal mesenchyme is not required for normal palatogenesis.

2 Results and Discussion

2.1 Expression of *Fgf18* in the developing palate and mandible

Fgf18$^{-/-}$ mutant mice died shortly after birth, with most having a cleft palate defect.[9,10] To investigate the function of Fgf18 in palate development, we examined the expression patterns of *Fgf18* mRNAs during palate development in mouse embryos by using whole mount and section in situ hybridization analyses (Figure 1). *Fgf18* mRNA expression was observed in the posterior region of the developing palatal primordia at E11.5 (Figure 1A–E). From E12.5 to E13.5, the expression of *Fgf18* mRNAs was maintained at a high level in the posterior region of PS, and was decreased by E14.5 (Figure 1F–T). Compared with strong expression in the posterior region, *Fgf18* mRNA expression in the anterior regions of PS was at a much lower level in E12.5 and E13.5 embryos (Figure 1F, K). No *Fgf18* expression was detected in the middle region of PS (Figure 1A, F, K), consistent with previous report.[8] In addition to expression in the PS, *Fgf18* mRNAs were highly expressed in the developing tongue and mandible at E11.5 and E12.5 (Figure 1B–E, G–J), and in the maxillomandibular junction region at E13.5 (Figure 1M–O). These results suggest that Fgf18 signaling might regulate the development of multiple craniofacial structures during the time of palatogenesis.

2.2 Tissue-specific inactivation of *Fgf18* in premigratory neural crest cells caused cleft palate and micrognathia

Many of the craniofacial tissues expressing *Fgf18* are derived from cranial neural crest cells. The *Wnt1-Cre* transgenic mice express the Cre recombinase in premigratory neural crest cells and have been widely used in craniofacial development studies.[11,12] We crossed *Fgf18*$^{c/c}$ conditional mice with *Wnt1-Cre* transgenic mice to investigate the role of *Fgf18* expression in the neural crest-derived craniofacial mesenchyme. The *Fgf18*$^{c/c}$*;Wnt1-Cre* pups were born at expected Mendelian ratio but most of them died shortly after birth with an “air in stomach” phenotype. By morphological analysis and skeletal preparations at E18.5 and later stages (Figure 2), we found that ~64% (18 out of 28) of *Fgf18*$^{c/c}$*;Wnt1-Cre* pups exhibited CP (Figure 2F, L), which is a lower penetrance than previously reported for CP in *Fgf18*$^{-/-}$ mice.[9] A few *Fgf18*$^{c/c}$*;Wnt1-Cre* pups that didn’t have overt CP survived for a few days after birth but failed to thrive and died before weaning. Analyses of skeletal preparations of E18.5 embryos revealed that all *Fgf18*$^{c/c}$*;Wnt1-Cre* mutants, regardless whether they had CP, exhibited shortened lower and upper jaws compared with control littermates (Figure 2G–L). In addition, ossification of the frontal and nasal bone was decreased and the ossification of the presphenoid bone in the cranial base was severely impaired in the *Fgf18*$^{c/c}$*;Wnt1-Cre* mutants compared with their control littermates (Figure 2M–R). These data indicate that *Fgf18* expression in the neural crest-derived mesenchyme is crucial for craniofacial bone development.

We measured the lengths of lower and upper jaws of the skeletal preparations to quantify the micrognathia defect in the *Fgf18$^{c/c}$;Wnt1-Cre* mutants. No significant length difference of mandibular bone was found between *Fgf18$^{c/c}$;Wnt1-Cre* embryos with and without CP (Figure 2S, T). However, the length of the mandibular bone was reduced by 14.5%, whereas the length of the upper jaw, measured from the posterior edge of the basisphenoid bone to the anterior end of the nasal cartilage (Figure 2J), was reduced by 5.9%, in the *Fgf18$^{c/c}$;Wnt1-Cre* embryos compared with control littermates at E18.5 (Figure 2S, T). These results indicate that *Fgf18* expression in the neural crest-derived mandibular mesenchyme plays a crucial role in mandibular growth.

In addition to cleft palate, high arched palate (also described as high-vaulted palate), which is characterized by an abnormally pronounced curvature angled superiorly along the palatal midline, is another palatal anomaly associated with many craniofacial syndromes.[13–15] Patients with several FGF receptor hyperactivation syndromes, such as Apert and Pfeiffer syndromes, exhibit either cleft palate or high arched palate.[14] Despite the fused secondary palate, high arched palate is associated with postnatal upper airway obstruction and secondary dental anomalies, including gingival swelling and dental crowding, which significantly affect the quality of life.[14,15] Since those *Fgf18$^{c/c}$;Wnt1-Cre* mutant mice that were born without cleft palate defect failed to thrive postnatally, we examined whether those mutants exhibited high arched palate using a recently described quantitative method for defining high arched palate in mutant mice.[13] Both the palatal arch height and angles in the non-cleft *Fgf18$^{c/c}$;Wnt1-Cre* mutant pups were slightly increased but statistically not significantly different from those in the control littermates (n = 3 for each genotype) (Figure 3A–C). These results indicate that *Fgf18* expression in the neural crest-derived cranial mesenchyme does not play a crucial role in post-fusion palatal morphogenesis.

2.3 *Fgf18$^{c/c}$;Wnt1-Cre* embryos exhibited defects in palatal shelf elevation but no defect in palatal shelf growth

To investigate the mechanism of cleft palate pathogenesis in *Fgf18$^{c/c}$;Wnt1-Cre* embryos, we performed histological analysis of *Fgf18$^{c/c}$;Wnt1-Cre* embryos and their control littermates at different stages in palatogenesis (Figure 4). At E13.5, the *Fgf18$^{c/c}$;Wnt1-Cre* embryos exhibited similar PS shape and size to their control littermates (Figure 4A, B). By E14.5, whereas PS had elevated to the horizontal position above the tongue and began to fuse in control embryos (Figure 4C), *Fgf18$^{c/c}$;Wnt1-Cre* embryos exhibited failure of elevation of one or both PS (Figure 4D, E). At E16.5, when the control embryos showed complete palatal fusion with dissolution of the midline epithelial seam (Figure 4F), 60% (3 out of 5) of the *Fgf18$^{c/c}$;Wnt1-Cre* embryos exhibited cleft palate (Figure 4H, I), with some (1 of 5) still exhibited vertically oriented PS (Figure 4I).

Previous studies have shown that reduced palatal mesenchyme proliferation could cause the failure of PS elevation and fusion.[2,16] We examined whether cell proliferation was altered in the PS of *Fgf18$^{c/c}$;Wnt1-Cre* embryos at E13.5 by *in vivo* EdU labeling (Figure 5). However, no significant difference in palatal mesenchyme proliferation in any region of the PS was detected between *Fgf18$^{c/c}$;Wnt1-Cre* embryos and their control littermates (Figure 5A–G).

2.5 *Fgf18* expression in the palatal mesenchyme is not required for palatal shelf elevation and fusion

Since all *Fgf18$^{c/c}$;Wnt1-Cre* mutants exhibited significantly shortened mandible (Figure 2), a structural defect known to contribute to failure of PS elevation,[17,18] we investigated whether the mandible plays a key role in cleft palate pathogenesis in the *Fgf18$^{c/c}$;Wnt1-Cre* embryos by using the maxillary explant culture assay. Maxillary explants were manually dissected from fresh E13.5 *Fgf18$^{c/c}$;Wnt1-Cre* embryos and their control littermates and cultured in roller bottles as previously described.[18] After 3 days of culturing, 17 out of 20 (85%) *Fgf18$^{c/c}$;Wnt1-Cre* maxillary explants and 19 out of 22 (86%) control maxillary explants showed fused secondary palate (Figure 6A–D), with paired *t* test indicating no statistically significant difference between the mutant and control groups ($P = 0.36$). Histological analysis revealed that PS fusion was complete, with dissolution of the midline epithelial seam, in both *Fgf18$^{c/c}$;Wnt1-Cre* and control explants (Figure 6C, D).

Since we removed the mandible and tongue when performing the maxillary explant culture experiment and since Fgf18 was highly expressed in the developing tongue mesenchyme during the stages prior to PS elevation (Figure 1), we analyzed whether the tongue development was impaired in the *Fgf18$^{c/c}$;Wnt1-Cre* embryos. Histological analysis of E13.5 embryos showed no obvious difference in tongue shape or size in between the *Fgf18$^{c/c}$;Wnt1-Cre* embryos and their control littermates (Figure 7A, B). We measured the length and height of the tongue using serial midsagittal sections and found that there was no significant difference between the measurements from the *Fgf18$^{c/c}$;Wnt1-Cre* mutant and *Fgf18$^{c/+}$* control littermates (Figure 7C). Since FGF signaling, involving Fgf6 and Fgf10, has been implicated in playing important roles in myoblast proliferation, differentiation, and muscle organization during tongue morphogenesis,[19,20] we analyzed whether tongue muscle development was affected in *Fgf18$^{c/c}$;Wnt1-Cre* embryos by using immunofluorescent staining for muscle actin. Whereas the overall organization of the tongue muscles appeared similar in the E13.5 *Fgf18$^{c/c}$;Wnt1-Cre* mutant and *Fgf18$^{c/+}$* control littermates (Figure 7D–I), we consistently detected reduced muscle actin staining in the lateral sides of the superior longitudinal muscles in the anterior two-thirds of the tongue in the *Fgf18$^{c/c}$;Wnt1-Cre* embryos in comparison with the control littermates (n=3 each genotype) (Figure 7, compare H with E and I with F, respectively). Thus, *Fgf18* expression in the neural crest-derived tongue mesenchyme plays an important role in tongue muscle development and defects in both the mandible and tongue may contribute to the impairment of PS elevation in the *Fgf18$^{c/c}$;Wnt1-Cre* embryos.

To further verify whether *Fgf18* expression in the developing palatal mesenchyme plays a significant role in palatogenesis, we used *Osr2-CreKI* mouse line in which Cre expression was highly specifically activated in the palatal mesenchyme at the onset of PS outgrowth[21] to conditionally inactivate *Fgf18*. We first generated *Fgf18$^{c/c}$;Osr2-CreKI* mice and found that they survived postnatally and lived a normal life span. To ensure effective inactivation of *Fgf18* in the developing palatal mesenchyme, we crossed *Fgf18$^{c/c}$* mice to *EIIa-Cre* transgenic mice[22] and generated *Fgf18$^{+/-}$* heterozygous null mice. We then crossed *Fgf18$^{+/-}$* mice with *Fgf18$^{c/c}$;Osr2-CreKI* mice to analyze *Fgf18$^{c/-}$;Osr2-CreKI* progeny. Quantitative real-time PCR analysis of manually dissected PS tissues from E13.5 *Fgf18$^{c/-}$;Osr2-CreKI*

embryos showed that *Fgf18* mRNAs were decreased by 90% in the *Fgf18$^{c/-}$;Osr2-CreKI* mutant palatal tissues in comparison with the control littermate palatal tissues (Figure 8A), indicating efficient Cre-mediated inactivation of the *Fgf18* gene in the palatal mesenchyme. We found that *Fgf18$^{c/-}$;Osr2-CreKI* mice (n>20) were born at expected Mendelian ratio and lived without obvious growth or health problems. Histological sections of *Fgf18$^{c/-}$;Osr2-CreKI* embryos at E14.5 showed palatal fusion similar to control *Fgf18$^{c/+}$* embryos. These data indicate that *Fgf18* expression in the palatal mesenchyme is dispensable for palate morphogenesis, and that CP defects in *Fgf18$^{-/-}$* and *Fgf18$^{c/c}$;Wnt1-Cre* mutants were secondary consequences of other craniofacial structural anomalies such as micrognathia.

Recently, Hagan et al. (2019) generated a new *Fgf18* conditional mouse line, *Fgf18^{flox}*, in which the critical exon-1C is floxed,[23] whereas the *Fgf18^{c}* allele we used contained floxed exon-3.[24] They crossed the *Fgf18^{flox}* mice with *Dermo1^{Cre}* (also known as *Twist2^{Cre}*) mice, in which Cre is highly expressed in condensed mesenchyme including neural crest-derived cranial mesenchyme,[25] and showed that the *Dermo1^{Cre};Fgf18$^{flox/flox}$* mice exhibited calvarial and other skeletal defects similar to *Fgf18$^{-/-}$* mice but *Dermo1^{Cre};Fgf18$^{flox/flox}$* mutants did not have cleft palate.[23] It is not known whether *Fgf18* was effectively inactivated in the early mandibular and palatal mesenchyme in *Dermo1^{Cre};Fgf18$^{flox/flox}$* mutant embryos, however. Our results from the *Fgf18$^{c/c}$;Wnt1-Cre* and *Fgf18$^{c/-}$;Osr2-CreKI* mutants clearly demonstrate that *Fgf18* expression in the palatal mesenchyme is dispensable for palate morphogenesis. Hagan et al. (2019) also generated *Fgf18^{CreERT2}* knockin mice[23], which will be an excellent tool for lineage tracing *Fgf18*-expressing cells in cell-cell interactions during tissue morphogenesis, such as for further clarifying the role of Fgf18 signaling from the neural crest cells in tongue muscle morphogenesis.

3 Experimental Procedures

3.1 Mice

The previously described *EIIa-Cre*,[22] *Osr2-CreKI*,[21] *Wnt1-Cre*[11] transgenic mice and mice carrying the *Fgf18^{flox}* conditional allele[24] (abbreviated as *Fgf18^{c}*) were used in this study.

Since the *Wnt1-Cre* transgene was integrated in the *H2az2* locus,[26] which is located on the same chromosome as the *Fgf18* gene (mouse Chromosome 11), we first crossed *Fgf18$^{c/+}$;Wnt1-Cre* F1 male mice with CD1 female mice to generate *Fgf18$^{c/+}$;Wnt1-Cre* G2 male progeny that carried the *Wnt1-Cre* and *Fgf18^{c}* alleles in *cis*. Subsequently, we set up timed mating of *Fgf18$^{c/c}$* female mice with the *Fgf18$^{c/+}$;Wnt1-Cre* G2 male mice for analysis of *Fgf18$^{c/c}$;Wnt1-Cre* mutants and their littermates. In addition, *Fgf18$^{c/c}$* female mice were crossed with *EIIa-Cre* male mice[22] and the progeny crossed with C57BL/6 inbred mice to select for *Fgf18$^{+/-}$* mice carrying germline deletion of the floxed exon3 of the *Fgf18* gene for subsequent generation and analysis of *Fgf18$^{c/-}$;Osr2-CreKI* mice. For timed mating, embryonic day (E) 0.5 was designated as noon of the day when a vaginal plug was identified.

All animal work procedures were performed following recommendations in the Guide for Care and Use of Laboratory Animals by the National Institutes of Health and approved by the Institutional Animal Care and Use Committee (IACUC) at Cincinnati Children's

Hospital Medical Center. This study conformed with the ARRIVE guidelines (Animal Research: Reporting of *In Vivo* Experiments) for preclinical animal studies.

3.2 Histology, in situ hybridization, skeletal preparation, and immunofluorescent staining

Embryos and pups for histological analysis, *in situ* hybridization, and skeletal preparation were collected and processed as previously described.[27] Immunofluorescent staining of tongue muscles was performed with Anti-muscle Actin monoclonal antibody (1:1000, Clone HUC1–1, generously provided by Dr. James Lessard (Cincinnati Children's Hospital Medical Center).[28]) and goat anti-mouse secondary antibody (1:1000, Alexa Fluor® A11001, Lot#1484573, Life Technologies) on 8 μm- thick serial paraffin sections following the protocol described previously.[29] Images were taken using a Nikon DS-Qi2 microscope, and the autofluorescence of blood cells was removed with the image operations function of the NIS-Elements AR 4.30.03 64-bit software.

3.3 Cell proliferation analysis

Cell proliferation analysis was performed with minor modifications of the previously reported procedure.[18] Briefly, pregnant mice were injected intraperitoneally with EdU labeling reagent (Invitrogen Click-iT EdU Imaging Kit, 100 μL/mouse, 2.5 mg/mL in dimethyl sulfoxide [DMSO]) on the gestational day 13.5. One hour after injection, embryos were dissected, fixed in 4% PFA at 4°C overnight, embedded in paraffin, and sectioned at 5-μm thickness in the coronal plane. Immunodetection of EdU was carried out following the manufacturer's instructions. The numbers of EdU-labeled nuclei and total nuclei were recorded from 10 coronal sections each in the anterior, middle, and posterior regions of the PS from 3 pairs of control and mutant littermates. Data were recorded and measured using Nikon NIS-Elements AR 4.30.03 64-bit software. Student's *t* test was used to analyze differences in the data sets, and a *P* value less than 0.05 was considered statistically significant.

3.4 Quantitative real-time PCR

Total RNAs were extracted from manually dissected PS at E13.5 using the RNeasy micro kit (Qiagen, 74004). First-strand cDNAs were prepared using the SuperScript III First-Strand Synthesis System (Invitrogen, 18080–051), and real-time qPCR was performed using a Bio-Rad CFX96 Real-Time System with conditions recommended by the manufacturer. The relative levels of *Fgf18* mRNAs in each sample were normalized to that of *Hprt* mRNAs. Student's *t* test was used to analyze differential expression data. The sequences of *Fgf18* PCR primers are *Fgf18-E3-F* (CGAGGACGGGGACAAGTATG) and Fgf18-E4-R (GCCTTTTCGGTTCATACACAGG). The *Hprt* PCR primers used are *Hprt-F* (TGCTGGTGAAAAGGACCTCTCG) and *Hprt-R* (CTGGCAACATCAACAGGACTCC).

3.5 Embryonic maxillary explants culture

Embryonic maxillary explants were dissected from E13.5 $Fgf18^{c/+}$ and $Fgf18^{c/c}$;*Wnt1-Cre* embryos and cultured in roller bottles as previously described.[18]

3.6 Measurement of palatal arch height and angles

Palatal arch height and angle measurements were performed according to the method described by Conley et al (2016)[13] with minor modifications. Briefly, Embryos were dissected at E18.5, with the mandible and tongue removed from the embryonic heads. The samples were fixed overnight in 4% paraformaldehyde at 4 °C, and stained with the fluorescent DNA stain 4',6-diamidino-2-phenylindole (DAPI) in PBS. The stained samples were imaged using the Nikon FN1 upright MP confocal microscope, and 3D rendering was performed with NIS Element AR 5.200.00 64-bit software. The Palatal arch height measurements were obtained from Z-profiles via calculating the shortest distance from the highest superior point of the palatal arch (P_0 in Figure 3A) to the line connecting the lateral base of the palate shelves (P_1 and P_2 in Figure 3A). The line segments *a*, *b*, and *c* represent the distances from P_0 to P_1, P_0 to P_2, and P_1 to P_2, respectively, and the lengths of *a*, *b*, and *c* were measured with the NIS Elements AR 5.200.00 64-bit software. The height (*h*) was calculated using the formula

$$h = \frac{\sqrt{4a^2c^2 - \left(a^2 - b^2 + c^2\right)^2}}{2c}$$

The palatal angle (θ) was measured as the average of θ_1 and θ_2, which were calculated using the formulae $\theta_1 = \arcsin(h/a)$ and $\theta_2 = \arcsin(h/b)$. Student's *t* test was used to analyze differences in the data sets, and a *P* value less than 0.05 was considered statistically significant.

Grant Sponsors:

National Institutes of Health National Institute of Dental and Craniofacial Research grant DE027046; Shriners Hospitals for Children grant #85900.

Reference

1. Moxham BJ. The development of the palate: a brief review. Eur J Anat. 2003;7 (suppl. 1):53–74.
2. Bush JO, Jiang R. Palatogenesis: morphogenetic and molecular mechanisms of secondary palate development. Development. 1 2012;139(2):231–43. 10.1242/dev.067082. [PubMed: 22186724]
3. Lan Y, Jiang R. Sonic hedgehog signaling regulates reciprocal epithelial-mesenchymal interactions controlling palatal outgrowth. Development. 4 2009;136(8):1387–96. 10.1242/dev.028167. [PubMed: 19304890]
4. Rice R, Spencer-Dene B, Connor EC, et al. Disruption of Fgf10/Fgfr2b-coordinated epithelial-mesenchymal interactions causes cleft palate. The Journal of clinical investigation. 6 2004;113(12):1692–700. 10.1172/JCI20384. [PubMed: 15199404]
5. Jeong J, Mao J, Tenzen T, Kottmann AH, McMahon AP. Hedgehog signaling in the neural crest cells regulates the patterning and growth of facial primordia. Genes & development. 4 15 2004;18(8):937–51. 10.1101/gad.1190304. [PubMed: 15107405]
6. Han J, Mayo J, Xu X, et al. Indirect modulation of Shh signaling by Dlx5 affects the oral-nasal patterning of palate and rescues cleft palate in Msx1-null mice. Development. 12 2009;136(24):4225–33. 10.1242/dev.036723. [PubMed: 19934017]
7. Charoenchaikorn K, Yokomizo T, Rice DP, et al. Runx1 is involved in the fusion of the primary and the secondary palatal shelves. Developmental biology. 2 15 2009;326(2):392–402. 10.1016/j.ydbio.2008.10.018. [PubMed: 19000669]

8. Xu J, Liu H, Lan Y, Aronow BJ, Kalinichenko VV, Jiang R. A Shh-Foxf-Fgf18-Shh Molecular Circuit Regulating Palate Development. PLoS genetics. 1 2016;12(1):e1005769. 10.1371/journal.pgen.1005769. [PubMed: 26745863]

9. Liu Z, Xu J, Colvin JS, Ornitz DM. Coordination of chondrogenesis and osteogenesis by fibroblast growth factor 18. Genes & development. 4 1 2002;16(7):859–69. 10.1101/gad.965602. [PubMed: 11937493]

10. Ohbayashi N, Shibayama M, Kurotaki Y, et al. FGF18 is required for normal cell proliferation and differentiation during osteogenesis and chondrogenesis. Genes & development. 4 1 2002;16(7):870–9. 10.1101/gad.965702. [PubMed: 11937494]

11. Danielian PS, Muccino D, Rowitch DH, Michael SK, McMahon AP. Modification of gene activity in mouse embryos in utero by a tamoxifen-inducible form of Cre recombinase. Current biology : CB. 12 3 1998;8(24):1323–6. 10.1016/s0960-9822(07)00562-3. [PubMed: 9843687]

12. Debbache J, Parfejevs V, Sommer L. Cre-driver lines used for genetic fate mapping of neural crest cells in the mouse: An overview. Genesis. 6 2018;56(6–7):e23105. 10.1002/dvg.23105. [PubMed: 29673028]

13. Conley ZR, Hague M, Kurosaka H, Dixon J, Dixon MJ, Trainor PA. A quantitative method for defining high-arched palate using the Tcof1(+/−) mutant mouse as a model. Developmental biology. 7 15 2016;415(2):296–305. 10.1016/j.ydbio.2015.12.020. [PubMed: 26772999]

14. Stoler JM, Rosen H, Desai U, Mulliken JB, Meara JG, Rogers GF. Cleft palate in Pfeiffer syndrome. The Journal of craniofacial surgery. 9 2009;20(5):1375–7. 10.1097/SCS.0b013e3181ae42e4. [PubMed: 19816260]

15. Tabler JM, Barrell WB, Szabo-Rogers HL, et al. Fuz mutant mice reveal shared mechanisms between ciliopathies and FGF-related syndromes. Developmental cell. 6 24 2013;25(6):623–35. 10.1016/j.devcel.2013.05.021. [PubMed: 23806618]

16. Lan Y, Ovitt CE, Cho ES, Maltby KM, Wang Q, Jiang R. Odd-skipped related 2 (Osr2) encodes a key intrinsic regulator of secondary palate growth and morphogenesis. Development. 7 2004;131(13):3207–16. 10.1242/dev.01175. [PubMed: 15175245]

17. Li C, Lan Y, Jiang R. Molecular and Cellular Mechanisms of Palate Development. Journal of dental research. 10 2017;96(11):1184–1191. 10.1177/0022034517703580. [PubMed: 28745929]

18. Lan Y, Qin C, Jiang R. Requirement of Hyaluronan Synthase-2 in Craniofacial and Palate Development. Journal of dental research. 11 2019;98(12):1367–1375. 10.1177/0022034519872478. [PubMed: 31509714]

19. Hosokawa R, Oka K, Yamaza T, et al. TGF-beta mediated FGF10 signaling in cranial neural crest cells controls development of myogenic progenitor cells through tissue-tissue interactions during tongue morphogenesis. Developmental biology. 5 1 2010;341(1):186–95. 10.1016/j.ydbio.2010.02.030. [PubMed: 20193675]

20. Han D, Zhao H, Parada C, Hacia JG, Bringas P Jr., Chai Y A TGFbeta-Smad4-Fgf6 signaling cascade controls myogenic differentiation and myoblast fusion during tongue development. Development. 5 2012;139(9):1640–50. 10.1242/dev.076653. [PubMed: 22438570]

21. Chen J, Lan Y, Baek JA, Gao Y, Jiang R. Wnt/beta-catenin signaling plays an essential role in activation of odontogenic mesenchyme during early tooth development. Developmental biology. 10 1 2009;334(1):174–85. 10.1016/j.ydbio.2009.07.015. [PubMed: 19631205]

22. Lakso M, Pichel JG, Gorman JR, et al. Efficient in vivo manipulation of mouse genomic sequences at the zygote stage. Proceedings of the National Academy of Sciences of the United States of America. 6 11 1996;93(12):5860–5. 10.1073/pnas.93.12.5860. [PubMed: 8650183]

23. Hagan AS, Boylan M, Smith C, et al. Generation and validation of novel conditional flox and inducible Cre alleles targeting fibroblast growth factor 18 (Fgf18). Developmental dynamics : an official publication of the American Association of Anatomists. 9 2019;248(9):882–893. 10.1002/dvdy.85. [PubMed: 31290205]

24. Kimura-Ueki M, Oda Y, Oki J, et al. Hair cycle resting phase is regulated by cyclic epithelial FGF18 signaling. The Journal of investigative dermatology. 5 2012;132(5):1338–45. 10.1038/jid.2011.490. [PubMed: 22297635]

25. Goodnough LH, Dinuoscio GJ, Atit RP. Twist1 contributes to cranial bone initiation and dermal condensation by maintaining Wnt signaling responsiveness. Developmental dynamics : an official

publication of the American Association of Anatomists. 2 2016;245(2):144–56. 10.1002/dvdy.24367. [PubMed: 26677825]

26. Goodwin LO, Splinter E, Davis TL, et al. Large-scale discovery of mouse transgenic integration sites reveals frequent structural variation and insertional mutagenesis. Genome research. 3 2019;29(3):494–505. 10.1101/gr.233866.117. [PubMed: 30659012]
27. Liu Z, Li C, Xu J, et al. Crucial and Overlapping Roles of Six1 and Six2 in Craniofacial Development. Journal of dental research. 5 2019;98(5):572–579. 10.1177/0022034519835204. [PubMed: 30905259]
28. Sawtell NM, Lessard JL. Cellular distribution of smooth muscle actins during mammalian embryogenesis: expression of the alpha-vascular but not the gamma-enteric isoform in differentiating striated myocytes. The Journal of cell biology. 12 1989;109(6 Pt 1):2929–37. 10.1083/jcb.109.6.2929. [PubMed: 2687290]
29. Xu J, Liu H, Lan Y, et al. Hedgehog signaling patterns the oral-aboral axis of the mandibular arch. eLife. 1 14 2019;8. 10.7554/eLife.40315.

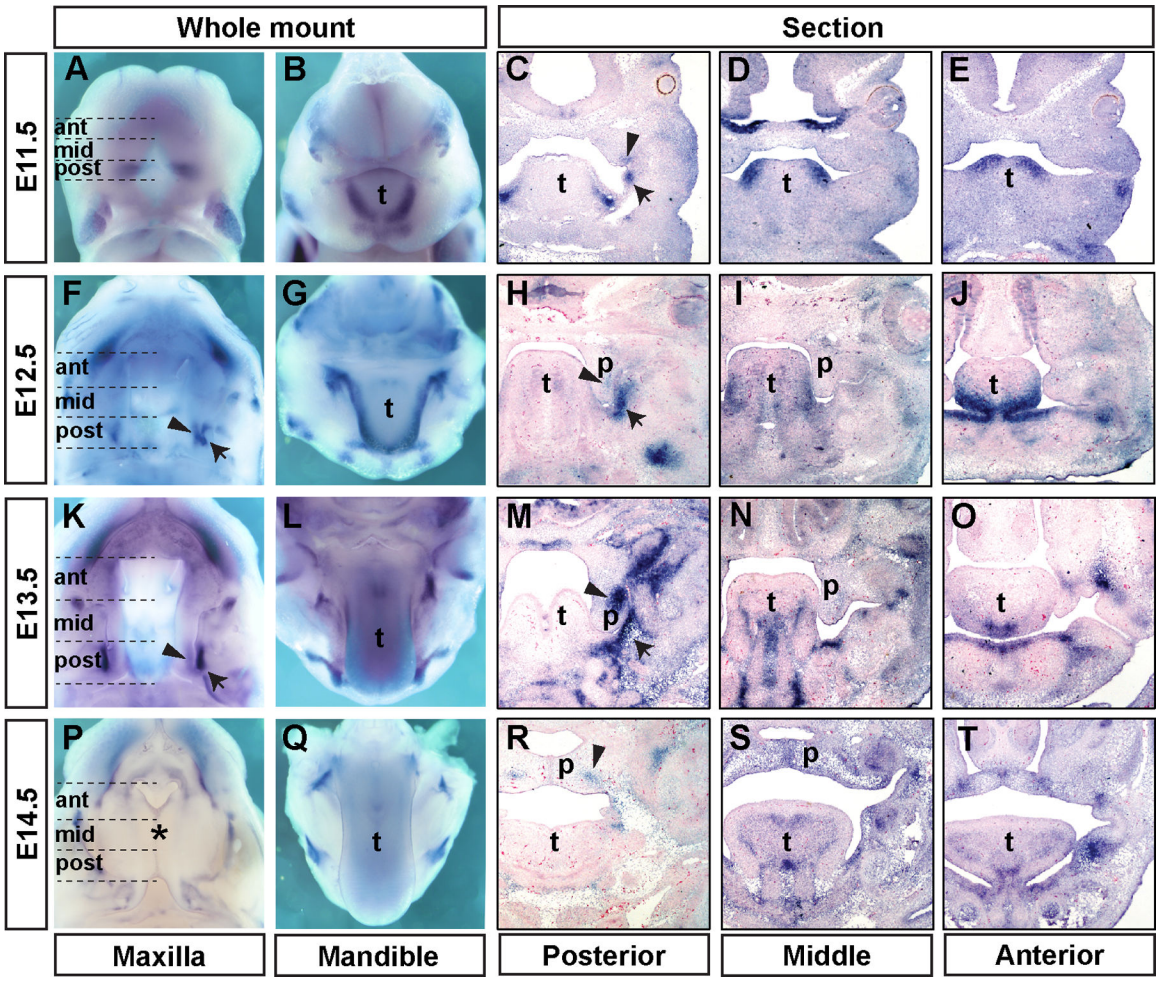

Figure 1. Patterns of *Fgf18* mRNA expression during palate development.

Whole-mount oral views of the upper and lower jaws (A-B, F-G, K-L, and P-Q) and frontal sections of mouse embryonic heads (C-E, H-J, M-O, and R-T) showing patterns of *Fgf18* mRNA expression in developing mouse craniofacial tissues at E11.5 (A-E), E12.5 (F-J), E13.5 (K-O), and E14.5 (P-T). Representative images of frontal sections from the posterior, middle, and anterior regions of the palatal shelves from each embryonic stage (the regions are indicated on whole mount images in the left column) are displayed from left to right in each row. Arrowheads point to the domain of *Fgf18* mRNA expression in the posterior palatal shelf. Black arrows point to the *Fgf18* expression at the maxillomandibular junction region, whereas green arrows point to the midline epithelial seam of the fusing secondary palate at E14.5. p, palatal shelf; t, tongue.

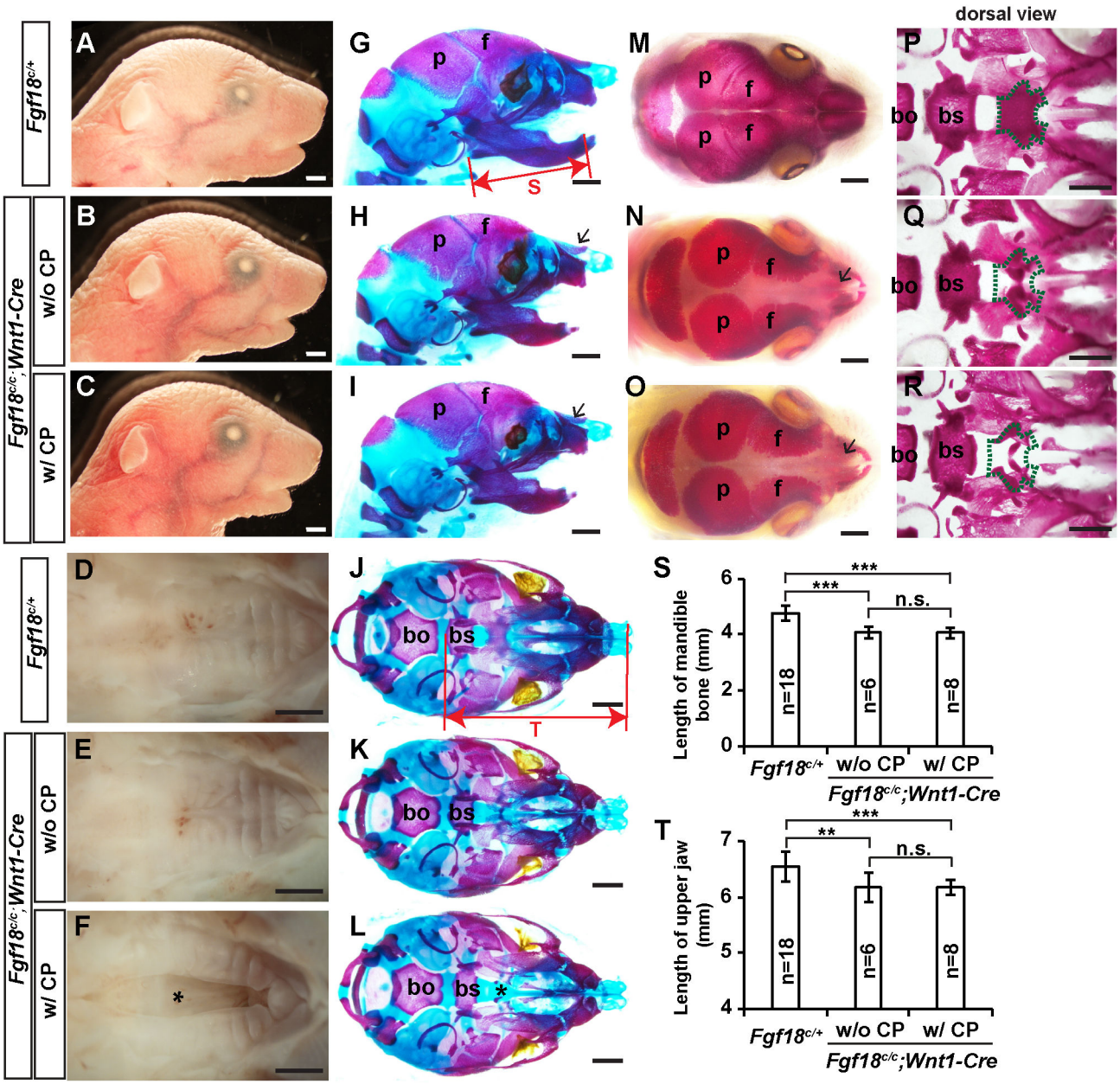

Figure 2. *Fgf18*$^{c/c}$*;Wnt1-Cre* mouse embryos exhibit micrognathia and cranial skeletal defects.

(A-F) Lateral (A-C) and palatal (D-F) views of P0 *Fgf18*$^{c/+}$ (A, D) and *Fgf18*$^{c/c}$*;Wnt1-Cre* (B, C, E, F) heads. (G-L) Skeletal preparations of E18.5 *Fgf18*$^{c/+}$ (G, J) and *Fgf18*$^{c/c}$*;Wnt1-Cre* (H, I, K, L) embryos were stained with Alizarin red and Alcian blue, with the lateral (G-I) and palatal (J-L) views shown. (M-R) Skeletal preparation of P0 *Fgf18*$^{c/+}$(M, P) and *Fgf18*$^{c/c}$*;Wnt1-Cre* (N, O, Q, R) pups were stained with Alizarin red only, with the dorsal views of heads (M-O) and the cranial base (following removal of the calvarial bones) (P-R) are shown. Arrows in H and L point to the underdeveloped nasal bones in *Fgf18*$^{c/c}$*;Wnt1-Cre* mutants. Green dashed lines in P-R show the position of the presphenoid bone. Asterisks in F and L mark the cleft palate. bo, basioccipital bone; bs, basisphenoid bone; f, frontal bone; p, parietal bone. (S and T) Quantitative comparison of the length of the mandibular

bone (G) and of the upper jaw (H). **, $P<0.01$; ***, $P<0.001$; n.s., no significant difference. Scale bar: 1 mm.

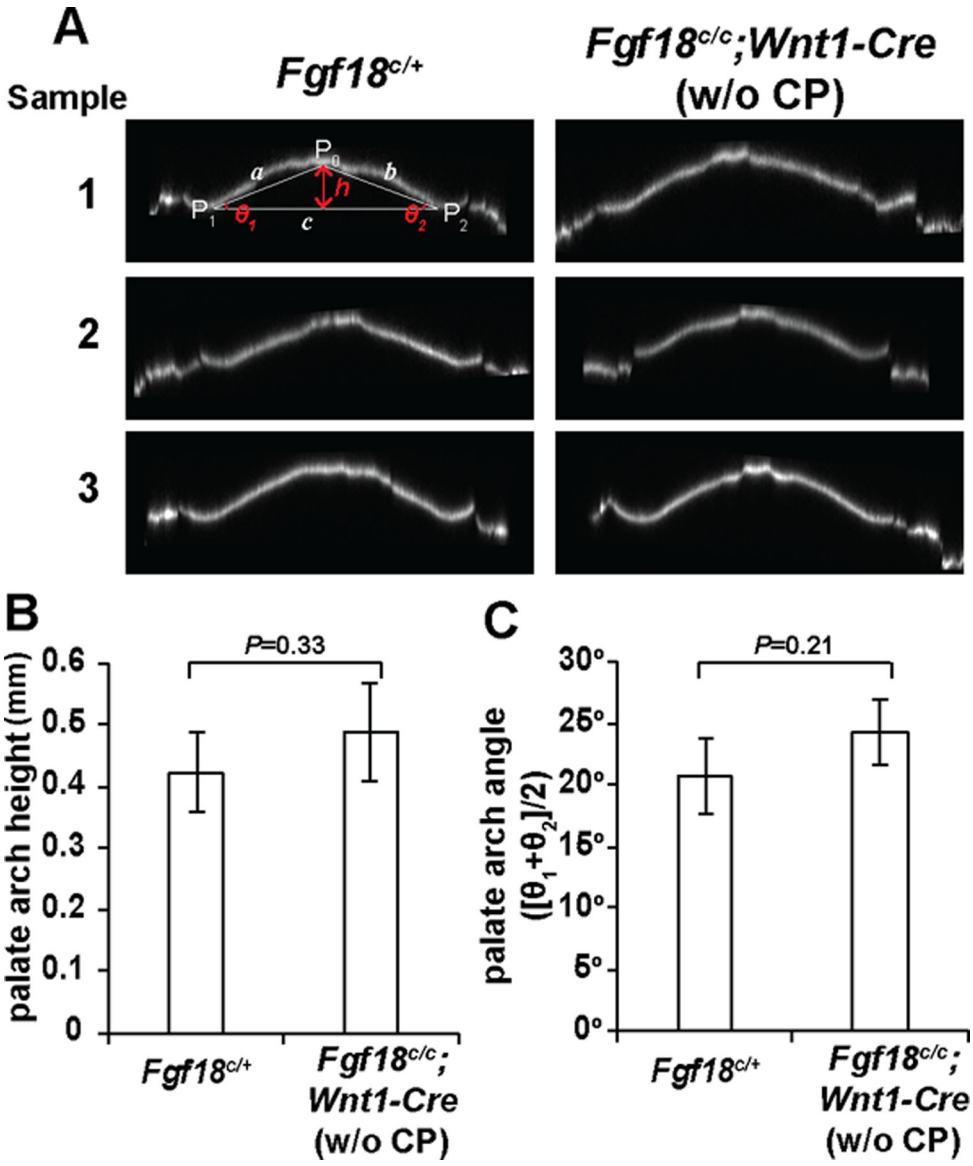

Figure 3. Analysis of palatal arch height and angles in *Fgf18*$^{c/+}$ and *Fgf18*$^{c/c}$*;Wnt1-Cre* embryos at E18.5.

(A-C) Z-profiles of corresponding maximum intensity projections of each embryo (A) and the statistical analyses of the palatal arch height (B) and angles (C). The formulae for calculating the length of the palatal arch height (*h*) and angles are described in the Experimental Procedures section.

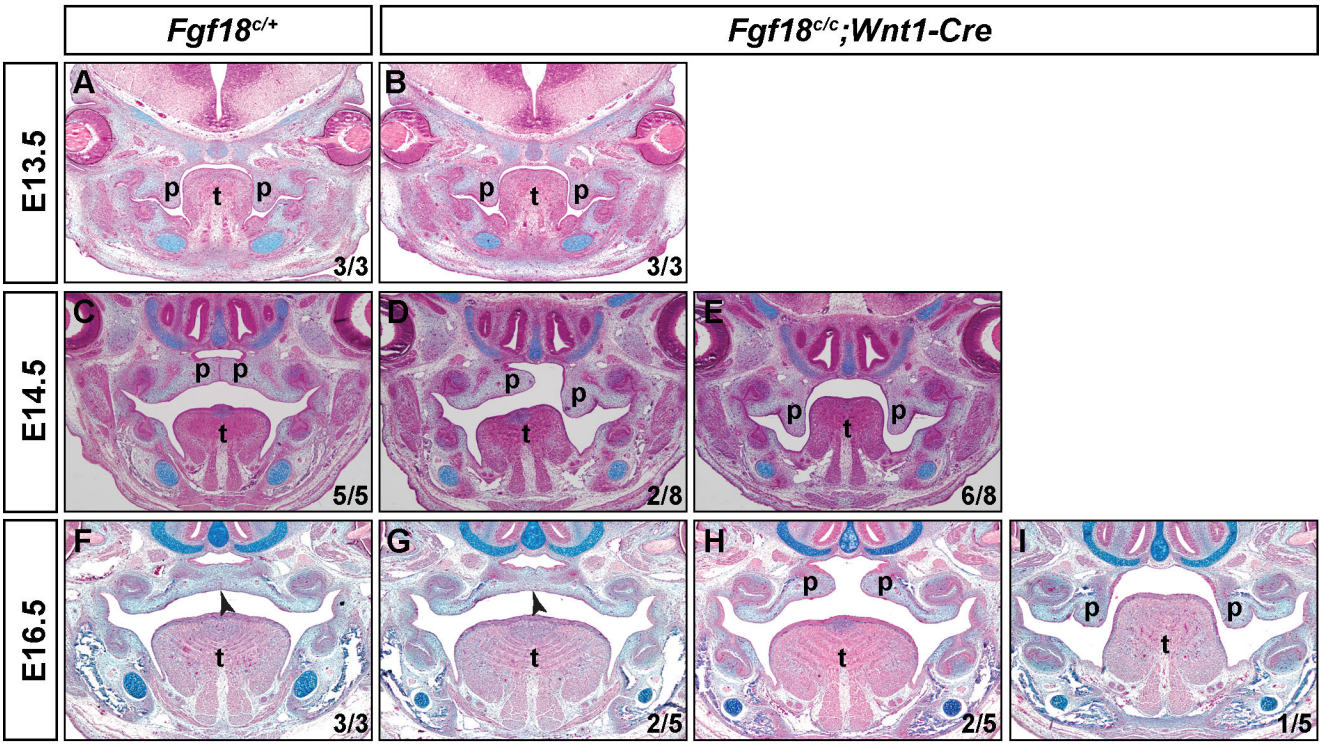

Figure 4. *Fgf18*$^{c/c}$*;Wnt1-Cre* mutant mouse embryos exhibited partial penetrance of cleft palate.

(A-I) Hematoxylin and eosin (HE) and Alcian blue-stained frontal sections from the middle region of the developing palatal shelves in *Fgf18*$^{c/+}$ and *Fgf18*$^{c/c}$*;Wnt1-Cre* embryos at E13.5 (A-B), E14.5 (C-E), and E16.5 (F-I). Arrowheads in F and G point to midline of the fused secondary palate. The ratio number in each panel indicates the number of embryos with the representative phenotype of total sectioned embryos of that genotype at that developmental stage. p, palatal shelf; t, tongue.

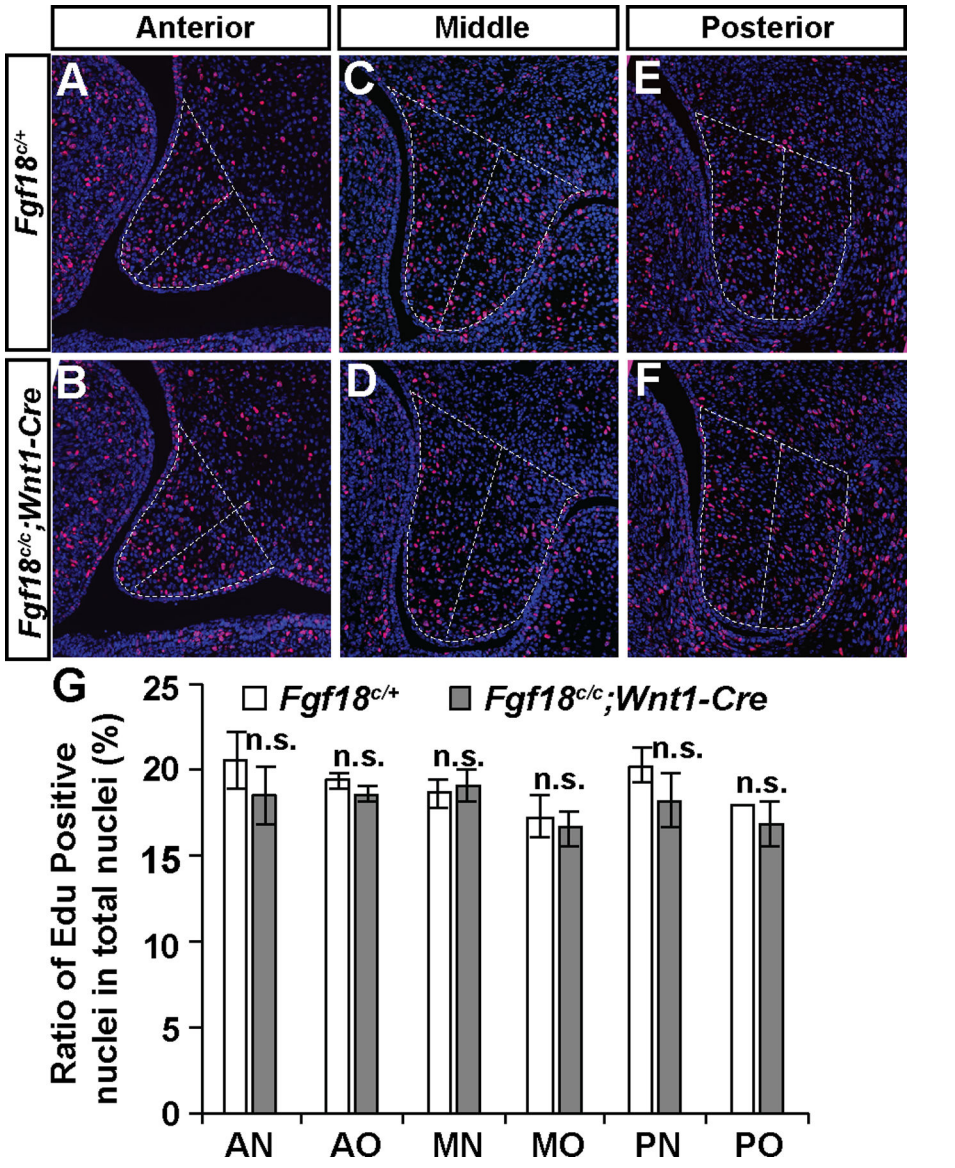

Figure 5. Analysis of palatal mesenchyme cell proliferation in *Fgf18*$^{c/+}$ and *Fgf18*$^{c/c}$;*Wnt1-Cre* embryos at E13.5.

(A-F) Representative images of frontal sections through the anterior (A, B), middle (C, D) and posterior (E, F) regions of the palatal shelves in E13.5 *Fgf18*$^{c/+}$ (A, C, E) and *Fgf18*$^{c/c}$ *Wnt1-Cre* (B, D, F) embryos showing the distribution of EdU-labeled nuclei (red). Sections were counterstained with DAPI (blue). The white lines divide the palatal shelf into oral and nasal sides for cell counts. (G) The percentage of EdU-labeled cells in the E13.5 palatal mesenchyme. Three embryos of each genotype were used for statistical analysis with Student's *t* test. AO, oral half of the anterior region; AN, nasal half of the anterior region; MO, Oral half of the middle region; MN, nasal half of the middle region; PO, oral half of the posterior region; PN, nasal half of the posterior region. n.s. no significant difference.

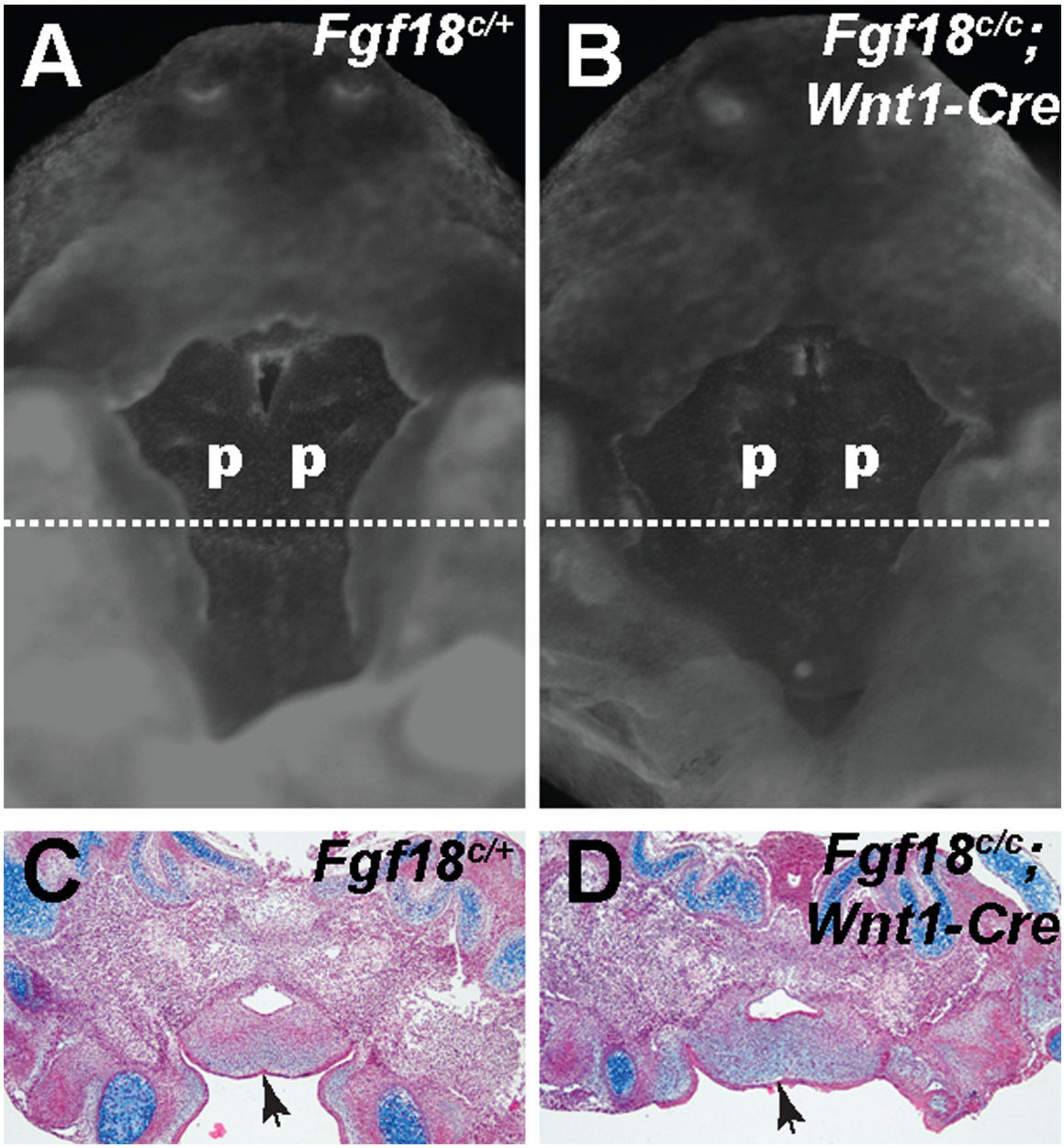

Figure 6. Analysis of palatogenesis in maxillary explants of E13.5 *Fgf18*$^{c/+}$ and *Fgf18*$^{c/c}$;*Wnt1-Cre* embryos.

(A-D) Whole-mount palatal view (A, B) and frontal sections through the middle region of the secondary palate (C, D) of the E13.5 maxillary explants after three days of organ culture *in vitro*. Dashed line in A and B indicates the approximate position of the frontal sections in (C) and (D). Arrow in C and D points to midline of fused secondary palate. p, palatal shelf.

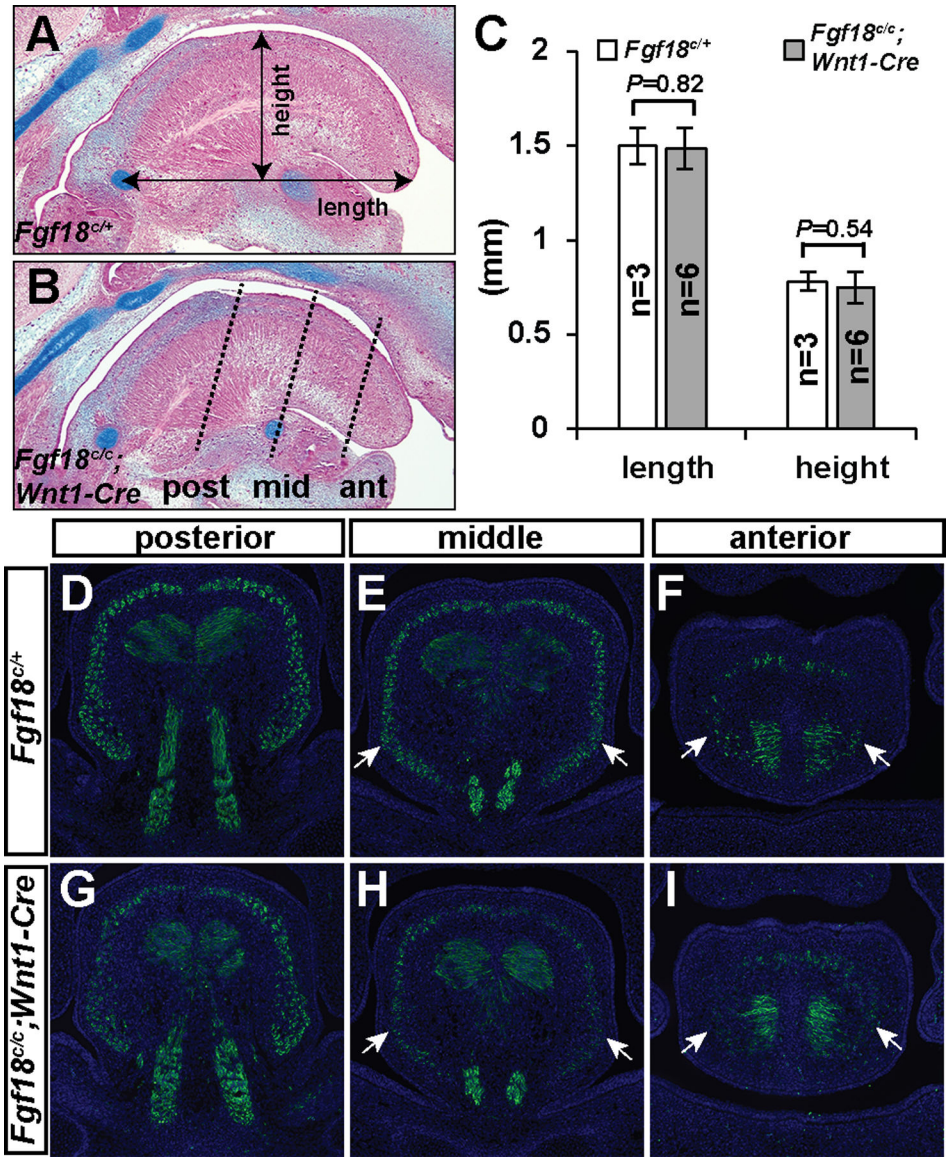

Figure 7. Analysis of tongue development in *Fgf18*$^{c/+}$ and *Fgf18*$^{c/c}$;*Wnt1-Cre* embryos at E13.5.

(A, B) Sagittal sections through the midline of the tongue in *Fgf18*$^{c/+}$ (A) and *Fgf18*$^{c/c;}$*Wnt1-Cre* (B) embryos at E13.5. Lines in (A) indicate the length and height measurement method. Dashed lines in (B) show the approximate positions of sections shown in (D-I). ant, anterior; mid, middle; post, posterior. (C) Quantitative comparison of the length and height of the tongue. (D-I) Immunofluorescent staining of muscle Actin (green) in *Fgf18*$^{c/+}$ (D-F) and *Fgf18*$^{c/c;}$*Wnt1-Cre* (G-I) embryonic tongue at E13.5. Sections were counterstained with DAPI (blue). White arrows point to lateral sides of the superior longitudinal muscle.

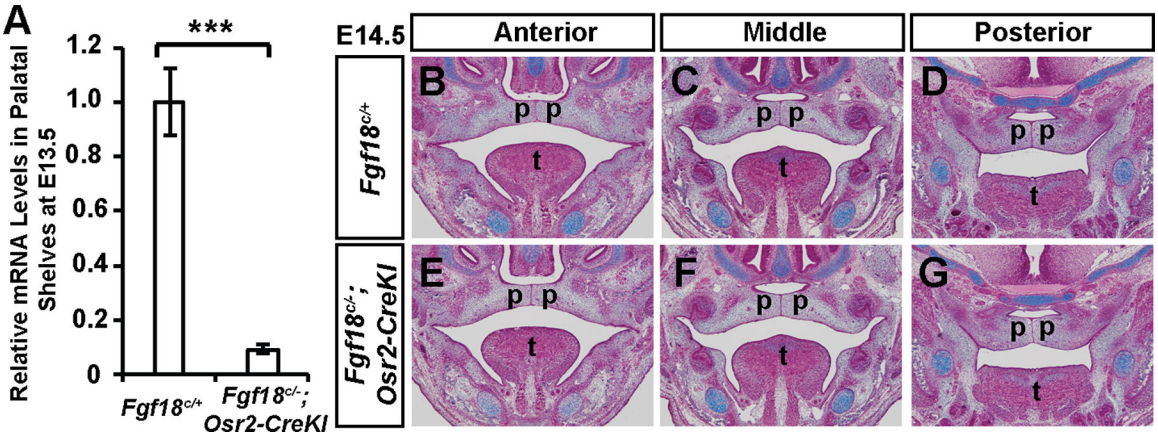

Figure 8. Palatal development occurred normally in *Fgf18$^{c/-}$;Osr2-CreKI* mutant embryos.

(A) Comparison of the of levels of *Fgf18* mRNAs in the palatal shelves of E13.5 *Fgf18$^{c/-}$;Osr2-CreKI* and *Fgf18$^{c/+}$* embryos by RT-qPCR analysis. ***, $P<0.001$. (B-G) Frontal sections through the secondary palate of E14.5 control (B-D) and *Fgf18$^{c/-}$;Osr2-CreKI* mutant (E-G) embryos at anterior (B, E), middle (C, F) and posterior (D, G) regions. p, palatal shelf; t, tongue.